Nuclear Magnetic Resonance Structure of the P395S Mutant of the N-SH2 Domain of the p85 Subunit of PI3 Kinase: An SH2 Domain with Altered Specificity†

Ulrich L. Günther,‡,§ Bernd Weyrauch,‡,§ Xinzhe Zhang,|| and Brian Schaffhausen*,||

Institute for Biophysical Chemistry, Centre of Biomolecular Magnetic Resonance, J. W. Goethe University, Frankfurt, Marie-Curie-Strasse 9, 60439 Frankfurt, Germany, and Department of Biochemistry, School of Medicine, Tufts University, 136 Harrison Avenue, Boston, Massachusetts 02111

Received March 4, 2003; Revised Manuscript Received July 21, 2003

ABSTRACT: Understanding the specificity of Src homology 2 (SH2) domains is important because of their critical role in cell signaling. Previous genetic analysis has characterized mutants of the N-terminal src homology 2 (SH2) domain of the p85 subunit of phosphoinositide 3-kinase (PI3K). The P395S mutant exhibits a specificity for phosphopeptide binding different from that of the wild-type SH2. The P395S mutant has an increased affinity for the platelet-derived growth factor receptor (PDGFr) compared to polyomavirus middle T antigen (MT). Solution structures of the P395S mutant of the p85 N-SH2 alone and complexed to a PDGFr phosphopeptide were determined to explain the change in specificity. Chemical shift perturbations caused by different peptides were compared for mutant and wild-type structures. The results show that the single P395S mutation has broad effects on the structure. Furthermore, they provide a rationale for the observed changes in binding preference.

Src homology 2 domains (SH2s)[1] are protein modules of approximately 100 amino acids that bind tyrosine-phosphorylated sequences (*1*−*4*). Both NMR and X-ray analysis have been used to determine the structure of a variety of SH2s (see ref *3* for a review). Generally, SH2s consist of a central antiparallel β-sheet flanked by smaller β-sheets and two α-helices. Peptide ligands bind approximately perpendicular to the sheet. Since there are almost 100 proteins that contain SH2s and many more that can be tyrosine-phosphorylated, specificity is an important issue. It has been known for a long time that ligand residues C-terminal to the phosphotyrosine, especially those at the +1 and +3 positions, are particularly important (*5*).

The SH2s of the p85 regulatory subunit of phosphatidylinositol 3-kinase (PI3K) are attractive models. Phosphatidylinositol 3-kinases are broadly important in cell function (*6*−*9*). They function in chemotaxis and phagocytosis (*10*). PI3K is important for organization of the actin cytoskeleton (*8*, *11*, *12*), in endosomal trafficking (*13*, *14*), and in cell migration (*15*). PI3K is also critically important for cell growth (*22*, *23*) and is strongly connected to oncogenic cell growth (*6*, *9*, *16*, *17*). Polyomavirus tumorigenesis is strongly dependent on the ability of the middle T (MT) oncogene to activate PI3K (*18*). PI3Ks can be grouped into three classes (*19*). The Ia enzymes are largely responsible for growth factor signaling and oncogenesis (*6*). These consist of heterodimers with a catalytic 110 kDa subunit and an 85 kDa regulatory subunit (*20*). The regulatory p85 subunit contains two src homology 2 (SH2) domains toward the C-terminal part of the molecule. These domains are responsible for interactions of PI3K with tyrosine-phosphorylated sequences of oncogenes such as middle T (*21*) or receptors such as the platelet-derived growth factor receptor (PDGFr) (*22*, *23*). The N-terminal SH2 of the wild type has been studied by both X-ray diffraction (*24*) and NMR (*25*−*27*). Deuterium exchange (*28*) and line broadening analysis (*29*) have been used to examine some of the dynamic properties of the domain. This previous work provides a foundation that permits careful examination of the behavior of mutant proteins.

The p85 N-SH2 was shown to bind pY[MVIE]XM sequences (*30*). In all SH2 structures, the ptyr binds in a hydrophobic pocket between the central β-sheet and the αA helix. For the p85 N-SH2, the residues involved in the coordination of the peptide were determined in X-ray structures (*24*) and by analyzing chemical shift perturbations for different ligands in HSQC spectra (*31*). The phosphate of ptyr is coordinated by the two arginines, R340 (αA2) and R358 (βB5). The ptyr+1 residue is bound on the central β-sheet with important interactions with K379 (βD3), I381 (βD5), and K419 (BG8). For a peptide with a V in ptyr+1, additional contacts to L420 (BG9) were observed. The BG loop undergoes a substantial rearrangement upon peptide binding, forming a hydrophobic pocket between the EF and the BG loop with many interactions with ptyr+3.

† This work was supported by the Deutsche Forschungsgemeinschaft, by the European Large Scale Facility for Biomolecular Magnetic Resonance in Frankfurt, Germany (UNIFRANMR), by NIH Grants CA34722 to CA50661 to B.S., and by a NATO collaborative research grant.

* To whom correspondence should be addressed. Phone: (617) 636-6868. Fax: (617) 636-2409. E-mail: brian.schaffhausen@tufts.edu.

‡ J. W. Goethe University, Frankfurt.

§ These authors contributed equally to this work.

|| Tufts University.

[1] Abbreviations: HSQC, heteronuclear single-quantum coherence; PDGFr, platelet-derived growth factor receptor; MT, polyomavirus middle T antigen; p85, 85 kDa subunit of phosphatidylinositol 3-kinase; PI3K, phosphatidylinositol 3-kinase, SH2, Src homology 2 domain; N-SH2, N-terminal src homology 2 domain of p85; ptyr, phosphotyrosine.

10.1021/bi034353x CCC: $25.00
Published on Web 08/30/2003

The work presented here is part of our ongoing effort to understand SH2 specificity. Specifically, it concerns a puzzle about SH2 specificity raised by previous genetic and structural analysis of the p85 N-SH2. Random mutagenesis produced a series of SH2 mutants with altered binding properties (*32*). Among these was the mutant P395S. This mutant was found to be defective in binding polyomavirus middle T antigen with its pYMPM binding sequence, while retaining its full ability to bind the platelet-derived growth factor receptor that has a pYVPM sequence. Residue 395, the position of the mutation, is located in the EF loop. In the wild-type protein, the side chain of P395 points away from the protein into the solvent. P395 is a trans isomer in the free and in complexes of the wild-type SH2. The EF loop is responsible for binding the ligand residue three residues C-terminal (+3) to the phosphotyrosine. Consistent with this, binding experiments with a degenerate peptide library showed a loss of binding specificity at the +3 position (*32*). While this explained the middle T defect, it did not explain why PDGFr remained fully active, since its residue at position +3 was methionine just like that of middle T. The binding experiments with the peptide library provided a biochemical explanation for this difference. While the wild-type N-SH2 most preferred to bind methionine at position +1, the P395S mutant exhibited a preference for valine. The PDGFr sequence is pYVPM; i.e., it has valine at position +1. This result suggested that loss of specificity at position +3 was compensated by an altered binding of the residue at position +1. Given models of SH2 function, this alteration of binding specificity is unexpected because the EF loop, where the mutation is located, is usually involved in the +3 and not the +1 interaction. This work examines the solution structure of the P395S mutant of the N-terminal SH2 of PI3K in its free state and bound to a peptide derived from PDGFr. In addition, effects on chemical shifts were compared for PDGFr and middle T peptides. The results show far-reaching effects of the point mutation and provide insight into the basis for the change in specificity.

MATERIALS AND METHODS

All samples of phosphorylated PDGFr peptide SVD-pYVPML-NH_2 and MT peptide EEEpYMPME-NH_2 were synthesized and HPLC purified by the Tufts Protein Chemistry Facility as described previously (*31*). The purity of the phosphorylated peptide was confirmed by HPLC. The N-SH2 of p85 (residues 321−434) was expressed in *Escherichia coli* as a pGEX 3X−glutathione *S*-transferase fusion. Protein samples were prepared as described previously (*27*, *31*) using 1 L of CELTONE-CN (MARTEK Biosciences Corp.). The concentration of the SH2 samples was approximately 1.5 mM. In the case of the complex, a reduced sample volume of 220 μL was used in a SHIGEMI NMR tube. NMR spectra were recorded at 500, 600, and 800 MHz. The chemical shift perturbations of NH resonances have been calculated according to the relation $|5\Delta(\delta^1H) + \Delta(\delta^{15}N)|$.

Sequential assignments for the P395S mutant SH2 alone and in a complex with a PDGFr peptide were originally obtained from ^{15}N-edited NOESY (*33*) and TOCSY (*34*) spectra and later confirmed by employing HNCA (*35*) and HN(CO)CA (*36*) spectra. Side chain assignments were primarily obtained from CC(CO)NH, HCC(CO)NH (*37*), and HCCH-TOCSY (*38*) experiments. Distance constraints were obtained from ^{15}N- and ^{13}C-edited NOESY (*33*) spectra recorded at 500, 600, and 800 MHz. In addition, dihedral angle constraints generated by the program TALOS (*39*) were used to calculate the structures in DYANA using chemical shifts from HCC(CO)NH and CC(CO)NH spectra.

For the assignment of the NOESY signals, NMR2ST (*40*) was used. This software compares peak lists from ^{15}N- and ^{13}C-edited NOESY spectra to the chemical shift values of assigned atoms and uses an existing structure as a starting point for the assignment of NOE signals. When multiple assignments were possible for one NOE signal, the structural distance for the assigned atoms is considered. For each filtering step, the obtained distance constraints were employed in a DYANA structure calculation (*41*). The calculated structures were then used for successive filtering steps to create new sets of distance constraints where the structural tolerances were set to 5 and 8 Å, respectively, for multiple assignments to enable variations from the given structure. After filtering had been carried out 10 times, the difference in the rmsd between structures of different iterations was smaller than 0.15 Å. Final assignments were verified by manual inspection.

Initial calculations for the protein complex included only intramolecular constraints. Intermolecular NOEs derived from ^{13}C{F1}-filtered two-dimensional (2D) NOESY spectra (*42*, *43*) were incorporated into the structure calculation after the protein fold had already converged in the absence of the ligand. All structures were energy minimized with MSI DISCOVER employing the final constraints obtained by the filtering process and manual inspection. Ramachandran plots and structural statistics were calculated employing PROCHECK (*44*).

RESULTS

Structure of the P395S Mutant SH2. Figure 1 shows the calculated structures for the P395S mutant in the absence of ligand. Figure 1A shows a bundle of the 20 best structures after distance geometry and energy minimization. The rmsd among these 20 structures is 1.76 ± 0.39 Å for all backbone atoms (N, C_α, and C′) and 2.92 ± 0.52 Å for all heavy atoms. The N-terminal part of the BG loop, the EF loop, and the BC loop are not well defined. If these areas are omitted from the rmsd calculation, values of 1.52 ± 0.31 Å for all backbone atoms are obtained. From ^{15}N- and ^{13}C-edited three-dimensional (3D) NOESY spectra 1113 distance constraints were found. This number is smaller that the 2225 constraints observed for the wild-type protein (*27*). The number of NOESY signals per residue is particularly low for residues in the BG and EF loops. This is reflected in the increased flexibility of the calculated structures in these regions. As for the wild-type protein, the BC loop is undefined because residues 361−365 could not be observed in any of our spectra. Eighty-five dihedral angle constraints predicted by TALOS were employed in the structure calculation. Examination of a Ramachandran plot created with PROCHECK (*44*) (not shown) indicated that 57.3% of the residues were in most favored regions, 30.3% in allowed regions, 6.7% in generously allowed regions, and 5.6% in disallowed regions. The residues that lie outside of the favored regions were in the undefined loop regions of the protein. The structural statistics are summarized in Table 1.

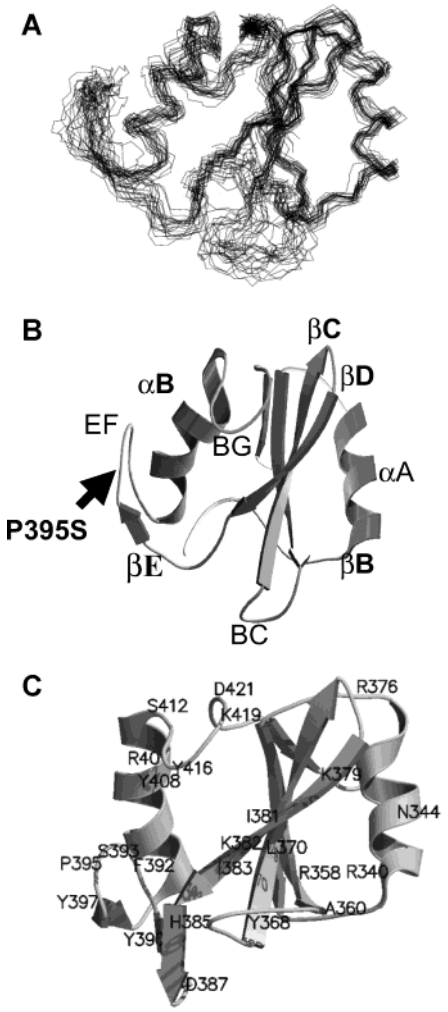

FIGURE 1: Structure of the P395S mutant SH2. (A) Bundle of the 20 best structures of P395S superimposed using the backbone atoms of residues 339−348, 353−360, 367−394, 402, and 413 for alignment. (B) Richardson diagram of the P395S mutant. (C) Richardson diagram of the wild-type p85 SH2. Residues discussed in the text are labeled.

The most important conclusion from the P395S structure is that the point mutation in EF causes significant changes in the structure extending quite far from the site of the mutation in the EF loop. The general shape of the core elements of the mutant structure (Figure 1B) is similar to that of the wild type shown in Figure 1C. The phosphotyrosine binding pocket is largely unaffected by the mutation. For example, all the C_α distances from the end of αA (residues 319−321) to the end of αB (residues 357−359) between the wild type and mutant are within 1 Å. Similarly, the βB and βC strands of the central sheet in the mutant showed no significant changes in their structure compared to the structure of the wild type. The structure of the uncomplexed mutant SH2 did show distinct differences from that of the wild type in the region of the hydrophobic binding pocket. βD has an extension (βD′) from N377 to R386. However, there is a change in the twist of βD′ that gives both I383 and F384 an altered position. F384 is rotated 90° in the mutant, and I383 thrusts more toward the hydrophobic pocket.

In contrast to the wild type, the EF loop region of the mutant shows no contacts to the rest of the structure. For example, contacts between the BG loop and the EF loop such as between F392 and Q415 observed for the wild-type protein were not seen in this mutant structure. Also, the stacking interaction between F392 and Y416 previously observed for the wild-type SH2 is missing in the P395S mutant. This loss of connectivity gives the BG loop an increased flexibility. αB is reoriented compared to the wild-type structure shown in Figure 1C (compare panels B and C of Figure 1). Where the αB helix in the wild type seems to splay away from the central sheet, in P395S it is oriented closer to the center of the molecule. The N-terminal bottom end of αB is slightly further away from the central sheet in P395S. The top C-terminal end of αB is closer to the central sheet. For example, residues Y408 and R409 are both closer to the central β-sheet in P395S (2.7 and 5.2 Å, respectively, from I381) than in the wild type. R409 is also rotated so that it is much closer to Y408 in the mutant than in the wild type.

There are also significant reorientations of the BG loop. As a consequence of missing contacts to EF, it is now closer to βD. The C_α distances from N377 at the top of βD to residues S412−K423 of BG are an average of 3.6 Å closer in P395S than in the wild type. Unlike the wild type, the side chains of K419 are now within 3 Å of both K379 and I381 in the mutant. As noted above, the ring of Y416 which was stacked with F392 in the wild type and closely connected with I381 in the wild type is no longer stacked or in close contact with those residues. L424 is much more exposed in the mutant structure.

Chemical Shift Differences between the Wild-Type Protein and the P395S Mutant. These structural changes were also reflected in chemical shift alterations compared to the wild-type protein. Figure 2A shows that the P395S point mutation causes significant (≥4 ppm) C_α chemical shift perturbations (csp) in eight residues and noticeable changes in several more. These changes were seen beginning in βD and continued through the BG loop. Among the residues strongly shifted are Y408 and R409, which were discussed above as

Table 1: Structural Statistics for the Structures of the Uncomplexed P395S Mutant and the P395S Mutant in Complex with the PDGFr Peptide

	uncomplexed	complexed
no. of distance restraints		
intramolecular ($i - j = 0$)	367	372
intermolecular ($\|i - j\| < 5$)	557	459
long-range ($\|i - j\| \geq 5$)	189	231
total	1113	1062
no. of dihedral angle restraints	85	91
rmsd of atomic coordinates (Å)		
residues 8−111		
backbone	1.76 ± 0.39	2.58 ± 0.65
all heavy atoms	2.92 ± 0.52	3.62 ± 0.66
residues 8−40 and 45−111		
backbone	1.64 ± 0.33	2.42 ± 0.68
all heavy atoms	2.79 ± 0.48	3.43 ± 0.67
residues 8−71 and 79−111		
backbone	1.67 ± 0.38	1.93 ± 0.36
all heavy atoms	2.78 ± 0.51	3.08 ± 0.47
residues 8−40, 45−71, and 79−111		
backbone	1.52 ± 0.31	1.67 ± 0.31
all heavy atoms	2.64 ± 0.47	2.82 ± 0.44
Ramachandran plot statistics (%)[a]		
residues in most favored regions	57.3	59.6
residues in additionally allowed regions	30.3	32.6
residues in generously allowed regions	6.7	5.6
residues in disallowed regions	5.6	2.2

[a] PROCHECK.

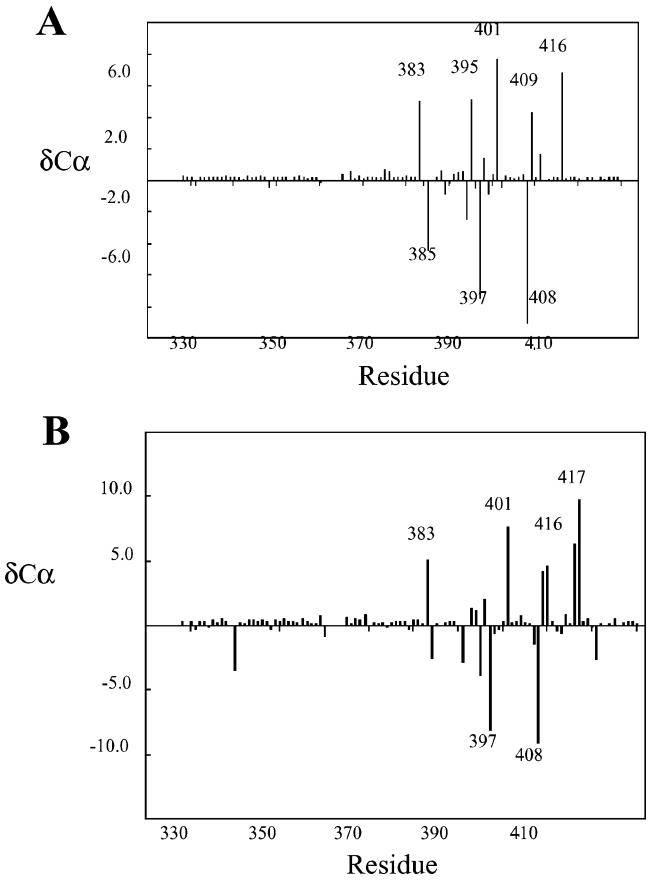

FIGURE 2: Chemical shift perturbations cased by the P395S mutation. (A) Chemical shift perturbation (csp) of C_α resonances of P395S compared to those of the wild type. (B) C_α chemical shift perturbations of the P395S mutant caused by binding the PDGFr ligand peptide.

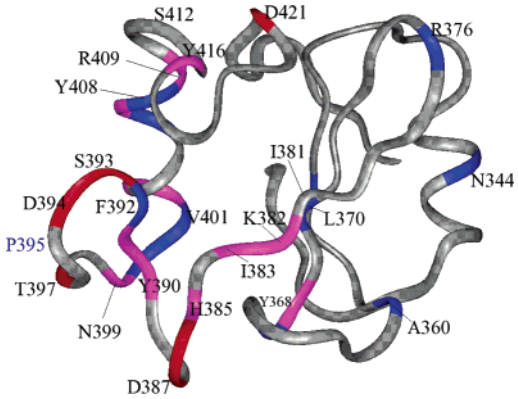

FIGURE 3: Mapping of NH chemical shift perturbations onto the P395S SH2 structure (*27*). Colors indicate chemical shift perturbations: blue for a csp's between 0.6 and 1.0 ppm, magenta for csp's between 1.0 and 2.0 ppm, and red for csp's above 2.0 ppm.

part of the change in αB. Also, Y416 is substantially shifted, probably because the stacking interaction with F392 is lost.

In Figure 3, residues with chemical shifts of backbone amides that are different than those of the wild-type protein are marked in three different colors: blue signals correspond to a csp between 0.60 and 1.0 ppm, magenta between 1.0 and 2.0 ppm, and red above 2.0 ppm. The point mutation caused changes even more widespread than those seen for the C_α chemical shifts. The most dramatic effects were observed for the resonances around the mutation site (shown in blue) where most NMR signals had to be completely reassigned. However, changes were observed from βC through the BG loop. In light of the structural result, it is not surprising that resonances of signals at the end of the αB helix and βD and βD′ have also been affected. For example, the NH resonances of V402, E403, H407, and R409 in the C-terminal end of αB were shifted by more than 1 ppm. Residues S400, V401, and N406 were shifted more than 0.8 ppm. In βD and βD′, K382, I383, H385, R386, and D387 were all shifted more than 1 ppm. In the BG loop, A414 and D 421 were strongly affected.

SH2−PDGFr Complex. Figure 4A shows the 20 best protein backbone structures for the P395S mutant SH2 complexed with the PDGFr peptide after distance geometry and energy minimization. The rmsd was 1.67 ± 0.31 Å for all backbone atoms and 2.82 ± 0.44 Å for all heavy atoms. A total of 1022 NOESY constraints and 91 torsion angle constraints predicted by TALOS were used in the structure calculation. For the unlabeled peptide ligand, 37 distance constraints (20 intermolecular and 17 intramolecular) were identified in $^{13}C\{F1\}$-filtered 2D NOESY spectra. A Ramachandran plot created with PROCHECK (not shown) showed that 59.6% of the residues were in most favored regions, 32.6% in allowed regions, 5.6% in generously allowed regions, and 2.2% in disallowed regions (Table 1). Figure 4B shows a Richardson diagram of the complex of the P395S SH2 with the peptide derived from PDGFr. The structure shows distinct differences compared to the structure of the uncomplexed P395S mutant. The residues in the EF loop could not be observed after ligand binding so there is no detailed information about their structure. The identification of protein−ligand interactions proved to be the most difficult part of this work. NOEs indicated with black labels in Figure 5 defined a network of contacts between the protein and the ligand. Because it was not possible to collect NOE data for the phosphate group, known contacts from the X-ray structure of the phosphate oxygens were incorporated into the DYANA structure calculations (Figure 5, red labels, and Table 2 of the Supporting Information). Distances from the X-ray structure of the wild-type SH2 (*24*) were set to 5 Å and those from ^{13}C-filtered NOESY spectra to 6 Å to leave sufficient flexibility in the structure calculation. The ligand binding sites can also be deduced from chemical shift perturbation studies. Ambiguous assignments from the NOE data were compared to the observed chemical shift perturbations.

In comparison to our previous structure for the wild-type SH2, the peptide backbone of the ligand crosses βD at a different position, around S380 rather than between I381 and K382. In looking at the overall structure of the mutant bound to ligand compared to its free form, we can see several changes. The N-terminal base of αB moves toward βD so that C_α atoms of S400 and V401 are approximately 4 Å closer to the C_α atom of I381 than in the free P395S structure. The C-terminal end of αB moves further away from βD so that the C_α atoms of residues 408−410 are 2.5−4.5 Å further away from I381 than in the free structure. The BG loop also generally moves outward, further away from βD. C_α of N417 which moves approximately 6 Å with respect to I381 is especially striking; Q415, Y416, and K419 also move more than 3 Å. A twist is imposed on βD by this movement.

Upon examination of the ligand binding, it appears that there are some differences in the phosphotyrosine coordina-

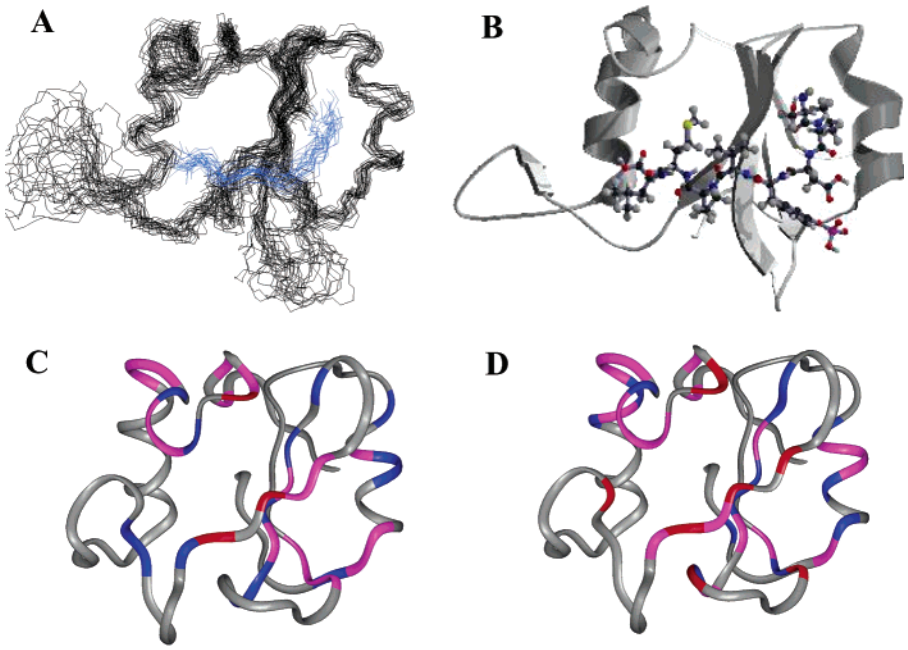

FIGURE 4: Structure of the P395S mutant SH2 in a complex with the PDGFr peptide. (A) Bundle of the 20 best structures of the P395S mutant protein in a complex with the SVDpYVPML-NH_2 peptide, derived from PDGFr (shown in blue). The structures were superimposed using the backbone atoms of residues 339−348, 353−360, 367−394, 402, and 413 for alignment. (B) Richardson diagram of the P395S mutant in a complex with a peptide derived from PDGFr. (C) Mapping of csp's caused by P395S SH2−SVDpYVPML-NH_2 (PDGFr) ligand binding on the SH2 structure: blue for csp's between 0.6 and 1.0 ppm, magenta for csp's between 1.0 and 2.0 ppm, and red for csp's above 2.0 ppm. (D) Mapping of csp's caused by P395S SH2−EEEpYMPME-NH_2 (MT) ligand binding on the SH2 structure: blue for csp's between 0.6 and 1.0 ppm, magenta for csp's between 1.0 and 2.0 ppm, and red for csp's above 2.0 ppm.

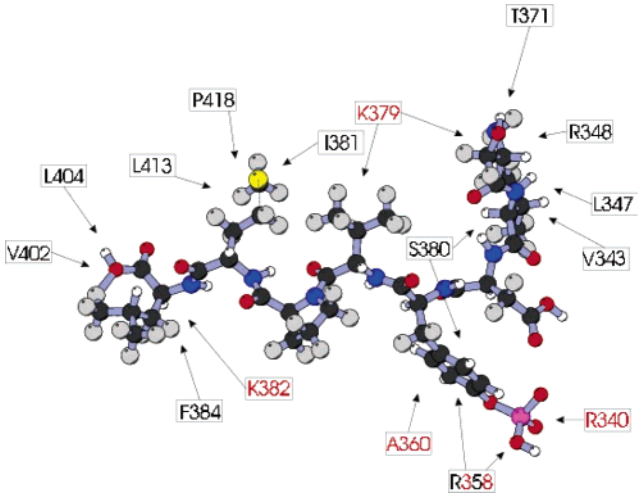

FIGURE 5: Side chain interactions of P395S with the SVD-pYVPML-NH_2 ligand peptide as revealed in 2D NOESY spectra (black labels). Additional constraints from an X-ray SH2 structure (red labels).

tion. A360 is involved in supporting the phenolic ring of the ligand ptyr. R340 of αA is noticeably further from the phosphate of the ptyr (5.76 vs 3.04 Å). There are also differences in the support for the phenolic ring. Most noticeably, K382 is much closer to the phenolic ring in the wild type (3.4 Å) than in the mutant (9.1 Å). The significance of these differences is unclear. Some variation in the fit of the ptyr has been noted in previous X-ray structures of a different variant of p85 (*24*). For example, depending on the ligand, R340 can be located 4.7−5.1 Å from the phosphate.

The P395S mutant SH2 has previously been shown to lack specificity at the +3 position of the ligand. This hydrophobic "pocket" appears to be much more open in the mutant than in the wild type. It is evident from the space filling models (Figure 6) that the methionine at position +3 is more exposed on the surface of the structure. The reason for this is primarily sequences in the BG loop (N417, K419, and L420) as well as F392 of the EF loop. In the P395S mutant, there are no close (<3 Å) contacts with F392 or K419 and fewer contacts with L420. The observed lack of specificity observed in the peptide fishing experiments probably results from this more open structure. However, contacts between the methionine at position +3 and βD (K379, S380, I381, and K362) as well as contacts with P418 and L420 in BG were observed in the structure. The contacts with I381, K382, and P418 were supported by the ^{13}C-filtered NOESY spectra. This supports the view that the binding of the residue at position +3, while nonspecific, contributes to the affinity for ligand binding.

The P395S SH2 has a strong preference for valine over methionine, where the wild type prefers methionine. This is the basis for the loss of affinity for middle T, while strong binding for PDGFr is retained. In contrast to the result for the methionine at position +3, the valine at position +1 appears to be more buried in the structure than the methionine at position +1 in the wild type. Interestingly, much of the difference seems to arise from the way the peptide is packed along the SH2 surface. pY, the residue at position +2, and the residue at position +3 contribute significantly to burying the residue at position +1. This packing of the residue at position +1 in the structure is affected by the fact that the ligand backbone crosses at a more N-terminal position of βD in the mutant than in the wild type. There is interaction with K379 (supported by NOESY signals) not seen in the wild type, and the packing with I381 is very different. The contact with K419 observed in the wild type is lost, because of both the change in the peptide position and changes in

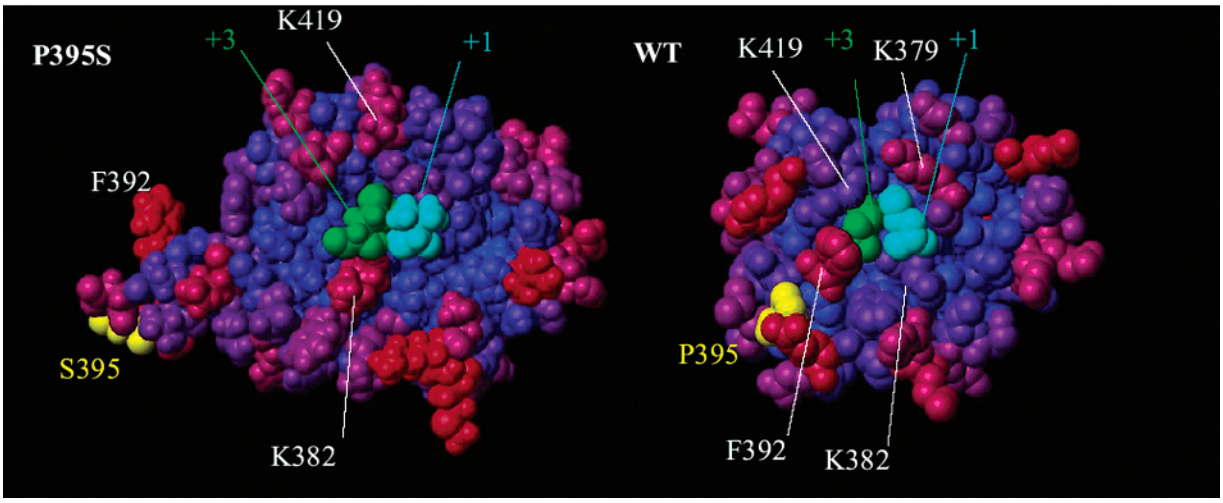

FIGURE 6: Space filling models of liganded wild-type (right) and P395S SH2 (left) showing the residue at position +1 in cyan and the methionine at position +3 in green. The mutation site is labeled in yellow. Color coding for all other residues represents increased solvent accessibility from blue to red.

the structure of BG. The arrangement of the peptide also positions the residue at position +2 differently. The edge of the proline ring is now close to K382. Since proline has not been used in the random peptide libraries, it is unclear whether this interaction contributes to specificity in a direct way.

Chemical Shift Perturbations of P395S upon PDGFr Peptide Binding. Figure 2B shows the chemical shift differences for C_α resonances between the free P395S mutant and the P395S mutant in a complex with SVDpYVPML-NH_2, the sequence derived from PDGFr. A large number of resonances were affected. The most prominent chemical shift perturbations were observed for R340 (−3.43 ppm), I383 (5.08 ppm), V401 (7.63 ppm), Y408 (−9.17 ppm), Y416 (6.26 ppm), and N417 (9.76 ppm). Other signals changing more than 1 ppm are those of F384 in βD, G391 and S393 in βE and EF, H407, R409, and N410 in the αB helix, and D421 in the BG loop. Shift changes of more than 0.5 ppm were observed for D337 before αA, D359 on βB, A360 and H365 flanking the BC loop, D367 and L404 in αB, and L413, A414, K419, and L425 in the BG loop.

In Figure 4C, the NH chemical shifts of the free P395S mutant are compared to those of the mutant complexed with the PDGFr peptide. As for wild-type SH2 (*31*), peptide binding resulted in broad chemical shift changes. The changes in chemical shifts in HSQC spectra upon ligand binding can be correlated to binding sites in the protein. Here we observed effects primarily in three regions of the protein: the ptyr binding site, the central β-sheet, and the BG loop. Residues 339, 340, and 358−360 show significant changes in their NH resonances where the ptyr is bound. The central β-sheet binds to valine at position +1, and there are also some interactions with the methionine at position +3. These were reflected in a change of the NH resonances of residues K379, S380, I381, and I383. The end of αB and the BG loop coordinates the +3 end of the ligand; changes in resonances for residues N410, E411, S412, Q415, Y416, K419, L420, and V422 were observed. Some chemical shift perturbations were also noted for residues in the αA helix as they bind the N-terminal region of the peptide ligand.

Chemical Shift Differences between the Free P395S Mutant and Its Complex with Polyomavirus Middle T Antigen (MT). Polyoma middle T binding to the P395S mutant is less effective than to binding to the wild type. Nonetheless, this ligand caused extensive changes in the chemical shifts of the P395S SH2 (Figure 4D). We observed chemical shift perturbations of >1 ppm for residues D339, N344, E345, K346, R358, A360, H365, D367, T369, L372, K379, I381, K382, I383, F384, R408, N410, E411, S412, Q415, Y416, N417, K419, L420, and L424 in HSQC spectra for the complex of the P395S mutant with the EEEpYMPME-NH_2 peptide, derived from MT. These changes include regions associated with binding of the ptyr, +1, and +3 residues.

DISCUSSION

Because of the numerous proteins that contain SH2s and the large number of potential tyrosine-phosphorylated targets, there has been much interest in understanding the basis for the specificity of SH2s. The goal of this work was to provide structural insight into the behavior of a mutant SH2 from PI3 kinase with altered specificity.

The P395S mutant poses an interesting structural question. How could a mutation in a surface loop involved in the coordination of the residue at position +3 cause a change in binding specificity for the residue at position +1? Compared to the wild type, the P395S SH2 mutant was defective in binding polyomavirus middle T antigen (pYMPM) but fully active in binding PDGFr (pYVPM). However, the mutation was in the EF loop that is expected to coordinate the +3 position. Indeed, in experiments with degenerate peptide libraries, P395S exhibited a loss of specificity at the +3 position after the ptyr (*32*). A biochemical basis for the change in specificity was found in the observation that P395S also exhibited a change in specificity at position +1 such that valine was now preferred over methionine. This compensation allows the mutant SH2 to continue to bind PDGFr with its pYVPM sequence as well as the wild type. Middle T with M at position +1 has no such compensation and so binds more weakly than to the wild type. Here structures have been determined for free P395S SH2 and an SH2−PDGFr peptide complex. In addition, chemical shift changes for wild-type and mutant SH2s have been compared. The results suggest satisfying explanations for the behavior of the mutant protein.

Geneticists concede that point mutations may have structural effects distant from the site of the mutation. Structural analysis of the P395 SH2 illustrates this point quite clearly. Although the single-amino acid change at position 395 occurs on a surface loop, the mutation has a much broader effect on the structure than just local changes in the EF loop. In contrast to previous wild-type structures, the EF loop has lost contacts to the rest of the structure. Specific interactions such as the stacking of F392 and Y416 are missing. The result is that βD of the central β-sheet, the αB helix, and the BG loop are all affected as well. BG is rearranged so that it is closer to the central β-sheet and more flexible. αB is reoriented so that it is closer to the central sheet. βD is twisted so that I383 and F384 are in different positions. I383 thrusts more toward the hydrophobic pocket. These structural differences between wild-type and mutant protein seen in the calculated structures were also reflected in the analysis of chemical shift perturbations for both C_α atoms and in the ^{15}N HSQC spectra. Changes could be seen from the central sheet through the EF loop and αB through the BG loop. Previous studies with peptide ligands altered at position pY, +1, or +3 have emphasized that the N-SH2 has a highly interactive structure (*31*). Alterations at position +1 affected residues of the +3 pocket and vice versa. The results with the P395S mutant again emphasize the highly interactive nature of the SH2 structure.

Once ligand binds, the P395S mutant undergoes significant structural change. Residues F392 and S395 of the EF loop could not be assigned. In fact, no detailed structural information about the EF loop could be obtained. The βD strand and the BG loop move apart as the ligand binds. The N-terminus of αB moves closer to the central sheet, while the C-terminus moves further away. These changes are also reflected in the large number of chemical shift perturbations when the ligand is bound to P395S. In this regard, the mutant behaved in a manner similar to that of the wild type in that it also exhibited many changes when ligand peptides were bound (*31*).

The real question is how these observations connect to the changes in specificity that are known to occur with the P395S mutant. The NMR results suggest that there are two causes of the loss of specificity at the +3 position. The methionine at position +3 of the PDGFr ligand is relatively exposed on the surface of the structure. This is much more reminiscent of the lack of contacts observed for the +2 position, which shows no specificity in the peptide fishing experiments, than it is of the +3 position in the wild-type complex for which the methionine side chain is much more buried in the structure. This exposure seems to have two sources. αB is closer to the central sheet which will alter the ability to pack the residue at position +3 into the structure. More importantly, the EF loop is not closing down on the residue at position +3, leaving a more open structure. However, the packing of the ligand is still tight as demonstrated by solvent accessibility calculations (Figure 6). In wild-type structures, F392 forms an edge coordinating position +3; in P395S, this residue remains a considerable distance away from that residue. The binding of ligand also resulted in the loss of the chemical shifts for residues in the region of the EF loop. Flexibility in this loop could accommodate a broader range of structures at position +3, resulting in the apparent lack of specificity. It is important to remember that despite the lack of specificity for the residue at position +3, that residue must contribute significantly to the overall affinity. The affinity of the MT peptide that exhibits a reduced level of binding is still significantly higher than that observed for a variant peptide in which the methionine at position +3 has been replaced with a glycine. Also, a number of significant contacts (K379, S380, I381, K362, and L420) between the residue at position +3 and the SH2 were observed.

Once it became apparent that the mutation caused substantial structural change, the altered preference (valine over methionine at position +1) became less surprising. The valine at position +1 is even more buried in the mutant SH2 structure than the methionine at position +1 is in the wild-type SH2. The methyl groups of Val at position +1 in the ligand interact with the hydrophobic surface formed by K379 and to a lesser extent I381 in βD. Examination of the structure suggests that, unless additional structural rearrangements were to occur, a methionine at position +1 with its longer side chain would expose a substantial hydrophobic surface to the solvent.

Examination of chemical shift changes for MT peptide binding also suggests a basis for the preference for valine at position +1 in P395S. Clear differences were seen in chemical shift changes for both the wild-type SH2 and the P395S mutant SH2 when the effects of the MT peptide are compared to that of the PDGFr peptide. Figure 7A shows the differences in csp's between the two peptides for the P395S mutant. We have previously shown that there are differences when each peptide binds to the wild-type SH2 (*31*). To understand why there is a relative loss of binding of the MT ligand, it is instructive to examine the differences in chemical shifts caused by the two ligands in P395S in comparison to the same differences in the wild-type structure (Figure 7B). It is worth noting that almost twice as many residues show strong differences (>0.6 ppm) in response to two ligands for the P395S mutant as for the wild type. Figure 7B summarizes differences $\{[(5\Delta\delta^1H + \Delta\delta^{15}N)_{MT\ peptide} - (5\Delta\delta^1H + \Delta\delta^{15}N)_{PDGFr\ peptide}]_{P395S\ SH2} - [(5\Delta\delta^1H + \Delta\delta^{15}N)_{MT\ peptide} - (5\Delta\delta^1H + \Delta\delta^{15}N)_{PDGFr\ peptide}]_{WT\ SH2}\}$ between the wild-type and mutant structures. F392 near the site of the mutation shows the largest difference. However, substantial differences were also observed in βB (H407 and Y408) and BG (A414, Y416, K419, and L420). It is this area of the structure that is likely responsible for the diminished level of binding of the middle T peptide with its methionine at position +1.

In summary, NMR structural analysis has been used to explain the behavior of a mutant SH2 that has altered specificity. The single P395S point mutation causes significant structural change in the SH2. Relaxed specificity at position +3 is associated with a more open structure that uses surface contacts rather than "burying" the side chain of residue +3. Altered selection at position +1 is associated with burying of the valine side chain in the peptide−SH2 structure. Chemical shift perturbations indicate that altered side chain interactions of a methionine at position +1 cause changes in the fit of the peptide elsewhere in the SH2. The issue of specificity can also be studied by kinetic analysis, which will be presented in detail elsewhere (T. Mittag et al. submitted for publication).

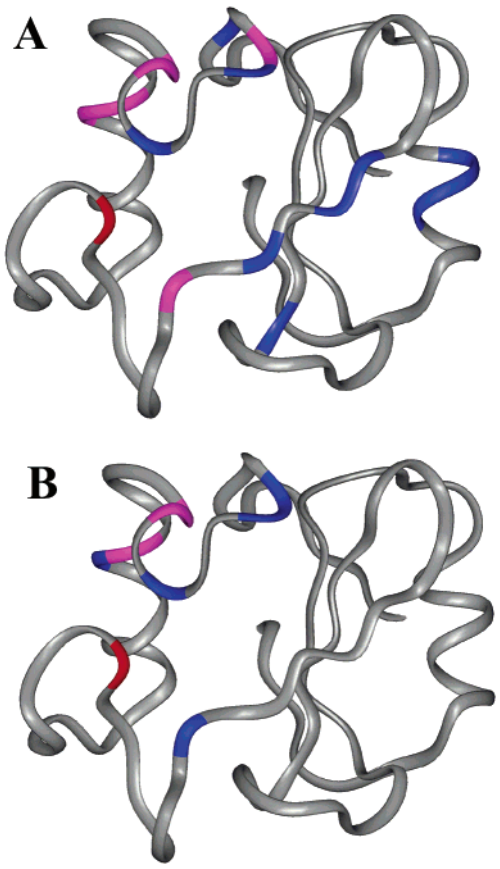

FIGURE 7: (A) Differences in csp's between MT and PDGFr binding $[(5\Delta\delta^1H + \Delta\delta^{15}N)_{MT\ peptide} - (5\Delta\delta^1H + \Delta\delta^{15}N)_{PDGFr\ peptide}]$ to P395S mapped on the SH2 structure: blue for csp's between 0.5 and 0.8 ppm, magenta for csp's between 0.8 and 1.5 ppm, and red for csp's above 1.5 ppm. (B) Comparison of the response of the wild type and P395S to different peptides. Differences between |csp(MT) − csp(PDGFr)| for P395 and |csp(MT) − csp(PDGFr)| for wild-type SH2. Coloring as in (A).

SUPPORTING INFORMATION AVAILABLE

Chemical shift perturbations and a table of constraints used in structure calculation. This material is available free of charge via the Internet at http://pubs.acs.org.

REFERENCES

1. Pawson, T., Gish, G. D., and Nash, P. (2001) *Trends Cell Biol. 11*, 504−511.
2. Schaffhausen, B. (1995) *Biochim. Biophys. Acta 1242*, 61−75.
3. Kuriyan, J., and Cowburn, D. (1997) *Annu. Rev. Biophys. Biomol. Struct. 26*, 259−288.
4. Cohen, G. B., Ren, R., and Baltimore, D. (1995) *Cell 80*, 237−248.
5. Cantley, L. C., and Songyang, Z. (1994) *J. Cell Sci., Suppl. 18*, 121−126.
6. Cantley, L. C. (2002) *Science 296*, 1655−1657.
7. Cantrell, D. A. (2001) *J. Cell Sci. 114*, 1439−1445.
8. Vanhaesebroeck, B., Leevers, S. J., Ahmadi, K., Timms, J., Katso, R., Driscoll, P. C., Woscholski, R., Parker, P. J., and Waterfield, M. D. (2001) *Annu. Rev. Biochem. 70*, 535−602.
9. Katso, R., Okkenhaug, K., Ahmadi, K., White, S., Timms, J., and Waterfield, M. D. (2001) *Annu. Rev. Cell Dev. Biol. 17*, 615−675.
10. Stephens, L., Ellson, C., and Hawkins, P. (2002) *Curr. Opin. Cell Biol. 14*, 203−213.
11. Wennstrom, S., Hawkins, P., Cooke, F., Hara, K., Yonezawa, K., Kasuga, M., Jackson, T., Claesson-Welsh, L., and Stephens, L. (1994) *Curr. Biol. 4*, 385−393.
12. Takenawa, T., and Itoh, T. (2001) *Biochim. Biophys. Acta 1533*, 190−206.
13. Backer, J. M. (2000) *Mol. Cell Biol. Res. Commun. 3*, 193−204.
14. Corvera, S. (2001) *Traffic 2*, 859−866.
15. Derman, M. P., Toker, A., Hartwig, J. H., Spokes, K., Falck, J. R., Chen, C. S., Cantley, L. C., and Cantley, L. G. (1997) *J. Biol. Chem. 272*, 6465−6470.
16. Vivanco, I., and Sawyers, C. L. (2002) *Nat. Rev. Cancer 2*, 489−501.
17. Dankort, D. L., and Muller, W. J. (2000) *Oncogene 19*, 1038−1044.
18. Freund, R., Dawe, C. J., Carroll, J. P., and Benjamin, T. L. (1992) *Am. J. Pathol. 141*, 1409−1425.
19. Domin, J., and Waterfield, M. D. (1997) *FEBS Lett. 410*, 91−95.
20. Carpenter, C. L., Duckworth, B. C., Auger, K. R., Cohen, B., Schaffhausen, B. S., and Cantley, L. C. (1990) *J. Biol. Chem. 265*, 19704−19711.
21. Yoakim, M., Hou, W., Liu, Y., Carpenter, C. L., Kapeller, R., and Schaffhausen, B. S. (1992) *J. Virol. 66*, 5485−5491.
22. Escobedo, J. A., Kaplan, D. R., Kavanaugh, W. M., Turck, C. W., and Williams, L. T. (1991) *Mol. Cell. Biol. 11*, 1125−1132.
23. Kashishian, A., Kazlauskas, A., and Cooper, J. A. (1992) *EMBO J. 11*, 1373−1382.
24. Nolte, R. T., Eck, M. J., Schlessinger, J., Shoelson, S. E., and Harrison, S. C. (1996) *Nat. Struct. Biol. 3*, 364−374.
25. Hensmann, M., Booker, G. W., Panayotou, G., Boyd, J., Linacre, J., Waterfield, M., and Campbell, I. D. (1994) *Protein Sci. 3*, 1020−1030.
26. Booker, G. W., Gout, I., Downing, A. K., Driscoll, P. C., Boyd, J., Waterfield, M. D., and Campbell, I. D. (1993) *Cell 73*, 813−822.
27. Weber, T., Schaffhausen, B., Liu, Y., and Gunther, U. L. (2000) *Biochemistry 39*, 15860−15869.
28. Shoelson, S. E., Sivaraja, M., Williams, K. P., Hu, P., Schlessinger, J., and Weiss, M. A. (1993) *EMBO J. 12*, 795−802.
29. Gunther, U., Mittag, T., and Schaffhausen, B. (2002) *Biochemistry 41*, 11658−11669.
30. Songyang, Z., Shoelson, S., Chauduri, M., Gish, T., Pawson, T., Haser, W., King, F., Roberts, T., Ratnofsky, F., Lechleider, R., Neel, B., Birge, R., Fajardo, J., Chou, M., Hanafusa, H., Schaffhausen, B., and Cantley, L. (1993) *Cell 72*, 767−778.
31. Gunther, U. L., Liu, Y., Sanford, D., Bachovchin, W. W., and Schaffhausen, B. (1996) *Biochemistry 35*, 15570−15581.
32. Yoakim, M., Hou, W., Songyang, Z., Liu, Y., Cantley, L., and Schaffhausen, B. (1994) *Mol. Cell. Biol. 14*, 5929−5938.
33. Driscoll, P. C., Clore, G. M., Marion, D., Wingfield, P. T., and Gronenborn, A. M. (1990) *Biochemistry 29*, 3542−3556.
34. Marion, D., Driscoll, P. C., Kay, L. E., Wingfield, P. T., Bax, A., Gronenborn, A. M., and Clore, G. M. (1989) *Biochemistry 28*, 6150−6156.
35. Ikura, M., Kay, L. E., and Bax, A. (1990) *Biochemistry 29*, 4659−4667.
36. Bax, A., and Ikura, M. (1991) *J. Biomol. NMR 1*, 99−104.
37. Kuboniwa, H., Grzesiek, S., Delaglio, F., and Bax, A. (1994) *J. Biomol. NMR 4*, 871−878.
38. Bax, A., Clore, G. M., and Gronenborn, A. M. (1990) *J. Magn. Reson. 88*, 425−431.
39. Cornilescu, G., Delaglio, F., and Bax, A. (1999) *J. Biomol. NMR 13*, 289−302.
40. Pristovsek, P., Ruterjans, H., and Jerala, R. (2002) *J. Comput. Chem. 23*, 335−340.
41. Guntert, P., Mumenthaler, C., and Wuthrich, K. (1997) *J. Mol. Biol. 273*, 283−298.
42. Gemmecke, G., Olejniczak, E., and Fesik, S. (1992) *J. Magn. Reson. 96*, 199−204.
43. Petros, A. M., Neri, P., and Fesik, S. W. (1992) *J. Biomol. NMR 2*, 11−18.
44. Laskowski, R. A., Rullmannn, J. A., MacArthur, M. W., Kaptein, R., and Thornton, J. M. (1996) *J. Biomol. NMR 8*, 477−486.

BI034353X